

Gas Transfer Between the Inner 3 kpc Disk and the Galactic Central Molecular Zone

YANG SU,^{1,2} SHIYU ZHANG,^{1,2} YAN SUN,^{1,2} JI YANG,^{1,2} FUJUN DU,^{1,2} MIN FANG,^{1,2}
QING-ZENG YAN,¹ SHAOBO ZHANG,¹ ZHIWEI CHEN,¹ XUEPENG CHEN,^{1,2} XIN ZHOU,¹ LIXIA YUAN,¹
AND YUEHUI MA¹

¹*Purple Mountain Observatory, Chinese Academy of Sciences, 10 Yuanhua Road, Nanjing 210023, China*

²*School of Astronomy and Space Science, University of Science and Technology of China, 96 Jinzhai Road, Hefei 230026, China*

ABSTRACT

We uncovered a more tilted molecular gas structure with highly negative velocities located near the dust lane. Our observations show that the approaching gas flows from the overshoot process are captured by the gravitational potential of the bar and then flow toward the Galactic central molecular zone (CMZ) through the bar channel. The recycled gas from the overshoot effect, in conjunction with freshly accreted gas from the inner 3 kpc disk, accumulates significantly near $R_{GC} \sim \frac{1}{2}R_{bar}$ and $R_{GC} \sim \frac{2}{3}R_{bar}$ regions by adopting a bar length of $\sim 3.2\text{--}3.4$ kpc. Importantly, within these regions, there are frequent collisions and substantial angular momentum exchanges between gas flows with different trajectories. In this scenario, the DISSIPATION processes arising from interactions between colliding flows, together with the varying torques induced by the nonaxisymmetric bar, effectively transfer the angular momentum of viscous gas outward, thereby driving the molecular gas to settle into the CMZ within about three orbital periods. A long-term gas inflow with an average rate of $\gtrsim 1.1 M_{\odot} \text{ yr}^{-1}$, coupled with intense transient accretion events that exceed the average rate by several times due to the overshoot effect, significantly regulates the gas distribution, physical properties, and dynamical evolution of the CMZ. These new findings provide robust observational evidence for elucidating the intricate dynamics of molecular gas flows toward the CMZ. Our observations suggest that gas dynamics have a significant impact on the secular evolution of both the Milky Way and the extragalactic gas-rich galaxies.

Keywords: Interstellar medium (847); Molecular clouds (1072); Galaxy kinematics (602); Milky Way Galaxy (1054); Galaxy structure (622); Milky Way dynamics (1051);

1. INTRODUCTION

The central molecular zone (CMZ), which may originate from the gas inflow driven by the

Galactic bar, hosts a huge amount of molecular gas (i.e., $2\text{--}6 \times 10^7 M_{\odot}$; Dahmen et al. 1998; Launhardt et al. 2002; Ferrière et al. 2007; Battersby et al. 2024) within $\sim 200\text{--}300$ pc of Sgr A*. As the closest observable galactic nucleus, the CMZ provides us with a wealth of

critical information about gas cycling in large-scale Galactic dynamics, star formation in extreme environments, and the various physical processes related to Galactic evolution (see the comprehensive reviews of Bryant & Krabbe 2021; Henshaw et al. 2023). Such studies on the Galactic CMZ are also of great significance for understanding the gas dynamics in other galaxies (e.g., the case NGC 1365 in Schinnerer et al. 2023), as well as the evolution of galaxies and their own nuclei (e.g., Leroy et al. 2021; Stuber et al. 2023; Schinnerer & Leroy 2024).

Molecular gas is the dominant gas component in the inner region of the Milky Way (e.g., Koda et al. 2016). Through spectral observations of molecular gas, we can investigate the distribution, kinematics, and other properties of molecular clouds (MCs) in detail. Although ^{12}CO does not reveal the internal density structure of MCs well, it is a good indicator of the extended structure of MCs and a useful tracer of the total mass of molecular gas. Additionally, the simultaneous observation of the ^{13}CO and C^{18}O lines can provide useful chemical information on MCs. By combining multiwavelength data from molecular gas and other tracers of stars, we are well placed to investigate the star formation in the Milky Way. So far, millimeter and submillimeter CO observations have been particularly important in studying molecular gas characteristics toward the Galactic CMZ.

Benefiting from the high-quality ^{12}CO and ^{13}CO data from the Milky Way Imaging Scroll Painting (MWISP) project (Su et al. 2019), Su et al. (2024) have identified many CO structures with unique morphological and kinematic features distributed along the major axis of the Galactic bar (see the Galactic stellar bar in, e.g., Wegg et al. 2015; Bland-Hawthorn & Gerhard 2016; Simion et al. 2017; Shen & Zheng 2020; Lucey et al. 2023; Vislosky et al. 2024). The bar channel traced by the CO dust lane connects the Galactic disk at the Galactocen-

tric distance of $R_{\text{GC}} \sim 3.2\text{--}3.4$ kpc and the CMZ at $R_{\text{GC}} \sim 0.3$ kpc. On the other hand, the length of the bar dust lanes is generally consistent with the radial scale length of the Galactic exponential disk (i.e., $\rho(R) \propto e^{-R/R_{\text{sl}}}$ and $R_{\text{sl}} \approx 3.2$ kpc, see Figure 13 in Su et al. 2021), likely indicating that the bar dynamics have a significant impact on the properties of the molecular gas in the inner Galaxy (e.g., distribution, morphology, kinematics, chemistry, and evolution). Our study provides solid evidence that the large-scale molecular gas inflow is driven by the Galactic bar toward the CMZ (see additional observations and simulations; e.g., Fux 1999; Rodriguez-Fernandez & Combes 2008; Sormani et al. 2015; Sormani & Barnes 2019).

The CO flows in the bar channel, driven by the nonaxisymmetric potential, become a secular and stable gas reservoir that feeds star formation in the CMZ and potentially supplies the supermassive black hole (SMBH) in the Galactic center (GC). The gas inflow rate onto the CMZ is estimated to be about $1.1 \pm 0.3 M_{\odot} \text{ yr}^{-1}$ in a transport period of ~ 24 Myr by adopting an average inflow velocity of $\sim 140 \text{ km s}^{-1}$ for the large-scale gas lane (Su et al. 2024). According to the MWISP CO data, the pattern speed of $\Omega_{\text{bar}} \lesssim 32.5 \pm 2.5 \text{ km s}^{-1} \text{ kpc}^{-1}$ supports that the Milky Way is currently in a slow-bar scenario, which is consistent with recent studies (e.g., Hilmi et al. 2020; Clarke & Gerhard 2022; Wheeler et al. 2022; Zhang et al. 2024a).

Despite much progress being made in multi-wavelength observations and numerical simulations, some open issues still need to be carefully investigated so that we can gain a more accurate understanding of the gas dynamics in the inner region of the Milky Way. How does the gas with significant angular momentum transfer from the Galactic disk several kiloparsecs away to the CMZ and even the GC? How are the molecular

gas fuels that subsequently form stars affected by the Galactic large-scale dynamics? What is the relationship between the gas inflow rate and the efficiency of the star formation in the CMZ? And what role do massive stellar winds, photoionization, radiation pressure, and supernova feedback play in the gas accumulation of the CMZ?

Our observations are instantaneous and freeze-frame. Can the observations accurately reveal the dynamical evolution of molecular gas flows toward the CMZ over time? In some specific studies, numerical simulations often simplify and discard many of the details of the large-scale gas flows in which the CMZ is embedded. Can some of the striking and interesting features in the simulations be verified by observations? In this paper, we investigate the dynamical nature of gas flows toward the CMZ based on the MWISP CO survey. Thanks to the large-scale MWISP data with high spatial resolution and sensitivity, we are able to capture many spatial and kinematic details of the molecular gas flow toward the CMZ that have never been revealed in previous studies.

In Section 2, we show that the tilted overshoot gas flows from the far dust lane converge in the near bar channel and eventually settle into the CMZ. In Section 3, a schematic diagram is constructed to illustrate both the overall dynamic behavior and detailed gas flow patterns toward the CMZ. We suggest that the dissipation processes resulting from collisions between large-scale gas flows are critical for removing the gas's angular momentum and facilitating its inward migration by considering the overshoot effect. In Section 4, we propose that the nonaxisymmetric gravitational potential of the bar plays a significant role in regulating the gas dynamics within 3 kpc of the Galaxy during its secular evolution. Finally, we give a summary in Section 5.

2. OVERSHOOT GAS FROM THE FAR DUST LANE

In Figure 1, the kinematic properties of the large-scale CO structures are well delineated toward the CMZ in the region of $l = [1^\circ 2, 16^\circ 2]$ and $v_{\text{LSR}} = [-120 \text{ km s}^{-1}, +300 \text{ km s}^{-1}]$. Besides the CO inflow driven by the Galactic bar (hereafter DL1; see the details in [Su et al. 2024](#)), two additional large-scale CO structures have been revealed flowing toward the CMZ along the near dust lane (i.e., DL2 and DL3; also refer to [Liszt 2006, 2008](#); [Sormani et al. 2019](#)). These gas flows are receding relative to the observer, so we identify them with red arrows in the l - v diagrams.

Unexpectedly, a new CO structure with the most negative velocity is discovered below the Galactic plane according to the large-scale MWISP data (the long blue arrow in the lower panel of Figure 1). The new kinematic CO structure consists of many filamentary MCs and exhibits a v_{LSR} gradient that increases with Galactic longitude. Obviously, the CO feature is not related to the near 3 kpc arm (see the long blue line in the lower panel of Figure 1; also refer to [Dame & Thaddeus 2008](#); [Reid et al. 2016, 2019](#); [Kumar et al. 2025](#)). On the contrary, the large-scale gas structure coexists with DL1 in a similar l - b range. More precisely, the approaching flow is roughly parallel to or slightly below the near dust lane (i.e., see the colors for the approaching gas and the white contours for the receding DL1 gas in Figure 2(c)). We define the large-scale approaching CO gas as the overshoot flows from the far dust lane (e.g., [Liszt 2006](#); [Wallace et al. 2022](#)).

In Figure 2(c), an intriguing filamentary cloud associated with the overshoot gas flow is found to be located in the G7 region ($l \sim 7^\circ 3, b \sim -1^\circ 1$) with a large velocity gradient of $\gtrsim +200 \text{ km s}^{-1} \text{ kpc}^{-1}$ by adopting a distance of $\lesssim 6 \text{ kpc}$ (see the parameters of the geometry in [Su et al. 2024](#)). The value is at least 2

times larger than the mean velocity gradient of the near dust lane (i.e., $\sim -100 \text{ km s}^{-1} \text{ kpc}^{-1}$ for DL1), indicating rapid deceleration of overshoot gas in the G7 region. The feature stems from the fact that the overshoot gas is undergoing strong tidal processes when it moves in the Galactic bar potential. As molecular gas flows pass through the apocenter of elongated elliptical orbits, MCs experience extremely strong torques and shear forces, resulting in significant geometric deformation from intense tidal effects (e.g., [Kruijssen et al. 2019](#)). Moreover, a considerable amount of overshoot gas is being pulled back by the Galactic bar potential and reenters the bar channel toward the CMZ, which is well delineated by the short blue arrows (OG1 and OG2) and the red arrows (DL2 and DL3) in Figure 1.

The overshoot flows are changing their trajectories in response to the Galactic bar potential, i.e., (1) from OG1 below the Galactic plane to DL2 above the plane (the upper panel of Figure 1) and (2) from OG2 at $b \sim -1.9^\circ$ to DL3 at $b \sim 0^\circ$ (the lower panel of Figure 1). Indeed, we distinctly illustrate that the large-scale multilayer shock structures with varying velocities are located in coherent but slightly different positions, indicating that the motion state of a series of overshoot flows with similar trajectories has changed dramatically in the vicinity of this region (see the shock structures indicated in blue, red, and green colors close to the G5 region at $l \sim 5.4^\circ$ and $b \sim -0.4^\circ$; Figure 2(a)). The data show that the overshoot gas is reaccelerating from $v_{\text{LSR}} \sim -40 \text{ km s}^{-1}$ to $v_{\text{LSR}} \sim +180 \text{ km s}^{-1}$ and even more at about half of the Galactic bar (i.e., at the middle of the near dust lane DL1 of $l \sim 5.7 - 4.9^\circ$ or $R_{\text{GC}} \sim 1.7 - 1.5 \text{ kpc}$) when it passes through the bar channel. The observations appear to be broadly consistent with the scenario of significant gas accumulation around the inner Lindblad resonance (ILR; e.g., $R_{\text{ILR}} \sim 1.6 \text{ kpc}$ in [Sormani et al. 2024](#)).

Collisions between gas flows are also revealed by observations. Combined with complementary distributions between the high-velocity gas (i.e., white contours for the DL2 inflows in Figure 2(b)) and the low-velocity overshoot gas (colors for the OG3 flows; also see Figures 6 and 7 in [Eden et al. 2020](#)), for example, the prominent CO protrusions evidently demonstrate that the two gas flows in opposite directions are colliding violently at the G3 region of ($l \sim 3.2^\circ$, $b \sim 0.3^\circ$). Interestingly, the receding gas of DL3 passing below G3 (see red color near $l \sim 3.4 - 2.9^\circ$, $b \lesssim 0.2 - 0.0^\circ$ in Figure 2(b)) also appears to collide with the surrounding overshoot gas, causing G3 to exhibit a deformed structure at ($l \sim 3.05^\circ$, $b \sim 0.15^\circ$). The observations are not only clear but also align well with the cloud–cloud collision scenarios discussed in the literature (e.g., see [Furukawa et al. 2009](#); [Inoue & Fukui 2013](#); [Gong et al. 2017](#); [Enokiya et al. 2021](#); [Fukui et al. 2021](#); [Williams et al. 2022](#); [Gramze et al. 2023](#)). According to the large-scale bow shock perpendicular to the dust lane in Figure 2(a), the G5 region at $R_{\text{GC}} \sim 1.6 \text{ kpc}$ is another excellent example of the collision between gas flowing along the bar channel (i.e., white contours for high-velocity receding gas in DL1) and the approaching overshoot flows passing through the bar channel (i.e., the blue and green colors for the low- and middle-velocity gas in OG2+DL3; also see [Akhter et al. 2021](#)). We believe that the approaching gas flows from overshoot are bombarding the large-scale receding gas streams in the vicinity of the near dust lane.

It is noteworthy that the large-scale shock structure near G5 (indicated by the yellow dotted line in Figure 2(a)) spans approximately 2.7° on the sky plane, corresponding to a projected physical size of about 320 pc at the distance of 6.8 kpc (see the geometry of the bar lanes in [Su et al. 2024](#)). Here, the size of $\sim 320 \text{ pc}$ may provide a reliable measurement

of the cross-sectional diameter of the bar channel, which is comparable to the size of the CMZ (e.g., see Henshaw et al. 2023). Indeed, the shock features (i.e., velocity jump) on the bar region can be well reproduced in simulations (e.g., Athanassoula 1992; Kim & Stone 2012; Feng et al. 2024). And our observations can provide additional constraints for hydrodynamic simulations of the Milky Way case. Potential signs of star formation are also observed near the apex boundary of the large-scale shock structure (see GMC M4.7-0.8 in Butterfield et al. 2025). This result may support the hypothesis that as the gas flow approaches the orbital apocenter (this work), the decrease in orbital velocity induces gas compression (density enhancement), thereby triggering localized star formation (Chaves-Velasquez et al. 2025). We propose that the strength of the inflowing gas, as well as gravitational potential (e.g., bar strength, axis ratio, and central mass distribution) and local interstellar medium properties (e.g., turbulence level, magnetic field strength, and star formation activity), influence the size and other properties of the Galactic CMZ.

At least two small breaks along DL1 can be identified in the l - v diagram (see the tips of OG1 and OG2 in the lower panel of Figure 1). The features can naturally be explained by the convergence of the overshoot gas from the far dust lane to the DL1 fresh gas from the $R_{GC} \sim 3$ –4 kpc region, leading discernible changes in the velocity gradient and gas distribution of the whole gas inflows along the near dust lane. The scenario is also consistent with the observational fact that lower-velocity overshooting gas is mainly concentrated upstream, while the higher-velocity DL1 gas becomes enhanced downstream (i.e., the slight displacement between the overshoot gas represented by the colors and the DL1 gas by white contours in Figure 2(c)). Moreover, the gradual velocity-shift features are indeed discerned along and/or

near OG1 and OG2 in the l - v diagrams (Figure 1). For the first time, our observations provide detailed evidence that large amounts of overshoot gas from the far dust lane are captured by the Galactic bar potential at these different R_{GC} and then inflow toward the CMZ along or parallel to the bar channel (e.g., DL2 and DL3).

According to the Gaussian decomposition and clustering algorithm (e.g., see Henshaw et al. 2019; Riener et al. 2019; Zhang et al. 2024b), we identified the MCs toward the CMZ by using the smoothing parameters of $\alpha_1=1.8$ and $\alpha_2=5.4$ for the MWISP ^{12}CO data with the 3D grid of $0.5' \times 0.5' \times 0.5 \text{ km s}^{-1}$. It is straightforward to pick out the DL1 samples from the near dust lane and the overshoot samples from the far dust lane based on the l - v diagrams (Figure 1). Accordingly, the intermediate samples are selected from MCs with v_{LSR} between the DL1 and the overshoot samples, i.e., MCs in DL2, DL3, G3, and G5 and near the head part of OG1, OG2, and OG3, excluding those from the blended regions. Table 1 displays the statistical properties of three types of MCs with angular sizes larger than 50 arcmin^2 .

By employing the method consistent with our earlier work (Su et al. 2024), we consistently derive the CO-to- H_2 conversion factor of $X_{\text{CO}} \sim 0.7 - 1.2 \times 10^{20} \text{ cm}^{-2} (\text{K km s}^{-1})^{-1}$. The value is about half of the commonly used value (e.g., Dame et al. 2001; Strong et al. 2004; Bolatto et al. 2013; Kohno & Sofue 2024) and close to $\sim (0.5 - 1.0) \times 10^{20} (\text{K km s}^{-1})^{-1}$ for the Galactic bulge region (e.g., Schultheis et al. 2014). Due to shocks driven by the bar and frequent cloud–cloud collisions, there may be multiple gas components with different temperatures and densities near the bar channel (e.g., Nilipour et al. 2024), resulting in systematic changes in the molecular gas state. Generally, in the strong shock and collision regions of G3 and G5, MCs with wide line broaden-

ings often have a relatively small ratio between ^{13}CO and ^{12}CO intensity, which is about half or less of the value of the normal MCs in the Galactic plane (e.g., $I(^{13}\text{CO})/I(^{12}\text{CO}) \sim 0.2$; see Tokuyama et al. 2019; Wang et al. 2023). The same is true of statistics for other gas flows associated with the Galactic bar (i.e., the large-scale MC samples with less contamination in the near dust DL1 and overshoot flows; see Table 1). Based on observations, the statistical result of the smaller $I(^{13}\text{CO})/I(^{12}\text{CO})$ likely represents the lower X_{CO} in the complex shock environments of the inner Galaxy.

The Milky Way represents an excellent case study for understanding gas cycling in galaxy evolution. Detailed observations have provided a wealth of data and information about the Milky Way, such as the 3D spatial distribution of gas flows, the precise geometric structure of the bar, and other relevant key physical parameters (e.g., the gas inflow rate, the outflow rate, the star formation rate in the CMZ, etc.). These detailed observational insights are crucial for constructing and constraining theoretical models, as they significantly advance our understanding of gas dynamics in galaxies and their secular evolution. Intriguingly, external galaxies also exhibit similar overshooting features (NGC 1097 and NGC 1365; see, e.g., Sormani et al. 2023; Whitmore et al. 2023; Schinnerer et al. 2023). Exploring the gas cycling processes and associated physical parameters (e.g., geometry of the bar and overshooting gas, distribution of gravitational potential, gas inflow rate, etc.) in external galaxies and comparing them with those in the Milky Way can elucidate the fundamental role of gas cycling in the broader context of galaxy evolution.

In summary, the molecular gas is a good indicator of the gravitational potential of the Galactic bar because the gas flows can be easily and quickly affected by the change in the gravitational torque of the rotating bar. The dynam-

ical processes dominated by the gravitational potential of the bar cause the overshoot gas to decelerate, accumulate, and collide violently at certain locations, systematically changing the gas motion and its overall distribution toward the CMZ. We propose that gas dynamics play a crucial role in studying several key issues, such as the redistribution of inflowing material and the regulation of overall gas inflow efficiency (Section 3), as well as the subsequent star formation efficiency in the CMZ (Section 4).

3. OVERALL DYNAMICS OF THE GAS FLOWS TOWARD THE CMZ

Using new data from the MWISP and supplements from other CO surveys (e.g., Dame et al. 2001; Tokuyama et al. 2019; Eden et al. 2020; Schuller et al. 2021), we construct a sketch to illustrate the overall dynamical nature and details of molecular gas flows toward the CMZ. The upper portion of Figure 3 displays an edge-on view of the spatial distribution and motion characteristics of the overall gas flows from the perspective of the observer, while the lower portion shows gas flows dominated by the Galactic bar’s gravitational potential in a face-on view. For the edge-on view, note that the gas inflows extend to $l \sim +16^\circ$ in the positive longitude (i.e., the near dust lane DL1; see Su et al. 2024) and $l \sim -8^\circ$ in the negative longitude for the far dust lane by assuming that it has a similar length and inclination angle of $\phi_{\text{bar}} = 23^\circ \pm 3^\circ$ (between the bar major axis and the Sun-GC) as DL1. The realistic scenario may be much more complex than what we depict here, but this sketch helps us get a comprehensive picture of the entire gas dynamics process toward the CMZ.

Many of the physical processes in the CMZ, including gas dynamics, have been studied in simulations, in which gas is compressed and shocked as a result of the shift from x1 orbit family to x2 orbit family (e.g., Athanassoula 1992; Englmaier & Gerhard 1999; Maciejew-

ski et al. 2002; Regan & Teuben 2004; Sheth et al. 2005; Rodriguez-Fernandez & Combes 2008; Combes et al. 2014; Sormani et al. 2015). As seen in Figure 3, our observations align well with the model in which the Galactic bar potential (1) channels a substantial amount of molecular gas from the inner Galactic disk at $R_{GC} \sim 3.2\text{--}3.4$ kpc toward the CMZ (i.e., DL1 and the associated kinematic features of CO gas), (2) generates noncircular motions and large-scale shock structures along the near dust lane (e.g., a series of bow shocks revealed by CO gas; Su et al. 2024), (3) governs and regulates the formation and evolution of the CMZ through the overshoot mechanism (i.e., gas flow collision/accumulation near G3/G5/G7 and multiple inflows DL2/DL3 with different trajectories toward the CMZ in Section 2; also see details in the following discussion), and (4) has important impacts on the gas distribution, properties, and subsequent star formation within the inner Galaxy (e.g., the 3 kpc arm, the thickness of the gas disk and the star formation rate therein, etc.). As another good example of gas influenced by the nonaxisymmetric bar potential, we will further discuss the tilted bar lanes traced by CO flows in Section 4.

The Galactic bar systematically transports a massive inflow toward the CMZ. However, this is a necessary but not a sufficient condition for the accumulation of gas in the CMZ. Another key question is how to effectively remove the large amount of angular momentum of the gas located a few kiloparsecs away, so that the gas can settle continuously into the region within the central few hundred parsecs of the Milky Way. Next, we will focus on how the overshoot effect plays a critical role in regulating the redistribution of gas and its angular momentum, as robustly evidenced by several key kinematic characteristics and dynamical effects observed in the new CO flows toward the CMZ.

In Section 2, we undoubtedly confirmed that G3 originates in violent collisions between the inflowing gas of DL2/DL3 and the overshoot gas from the far dust lane (the G3 case for x1 orbits intersects with x2 orbits; Figure 2(b)). In this way, G3 is located near the outskirts of the CMZ (i.e., at $R_{GC} \sim 0.5$ kpc). Meanwhile, gas flow collisions also occur in regions where the overshoot gas changes its trajectory and passes through the bar channel due to varying torques. When the overshoot gas enters the bar channel, collisions between gas flows are inevitable at the intersections of different eccentric orbits (the G5 and G7 cases for gas flow interactions in bar channel; Figures 2(a) and (c)). Therefore, collisions between gas flows are very common in extremely crowding orbits, especially in the region where the x1 orbits of gas intersect with the x2 orbits in nonaxisymmetric gravitational potential (Figure 3).

The starting points of DL2 and DL3 are located exactly around the regions of G7 and G5, respectively. And the gas mass in the intermediate samples is 1 order of magnitude higher than that in the overshoot gas, confirming significant accumulation of the overshoot gas within the bar channel at these certain locations (e.g., near the G7, G5, and G3 regions). The consistency may indicate that, due to the dynamics of the rotating bar, a significant accumulation of overshoot gas occurs in some special regions (i.e., near G5 at $R_{GC} \sim \frac{1}{2}R_{\text{bar}}$ and G7 at $R_{GC} \sim \frac{2}{3}R_{\text{bar}}$ by adopting the bar length of $\sim 3.2\text{--}3.4$ kpc; see Su et al. 2024). In addition, considerable CO emission in DL1 is also enhanced significantly near these regions ($l = 4^\circ 8' - 5^\circ 6'$ and $l = 6^\circ 9' - 8^\circ 3'$ in Figure 2(c); also see Figure 1 in Su et al. 2024). These regions are located near the apocenter of the overshoot flows (Figure 3). The interesting feature needs to be further explored.

Importantly, the measured line-of-sight velocities of the DL2 and DL3 inflows toward the

CMZ are ~ 1.5 – 8 times smaller than those of the DL1 at a similar R_{GC} (see Figure 1; also refer to the geometry proposed in Su et al. 2024). The observations clearly indicate that the tangential velocity of gas rotating clockwise around the GC has significantly decreased, and the orbital angular momentum of overshoot gas flows has been reduced by approximately 0.2–0.7 dex after being captured and reaccelerated by the bar potential. These features are consistent with the fact that there is substantial exchange of mass and angular momentum as overshoot gas changes from approaching flows to receding flows at some locations (e.g., the G7 region at ~ 2.2 kpc, the G5 region at ~ 1.6 kpc, and the G3 region at ~ 0.5 kpc; see Figures 2 and 3). Notably, our observations provide the first clear evidence that the overshoot gas, after being captured by the bar potential during its passage through the bar channel, continues to flow toward the CMZ with significantly reduced angular momentum.

The gas mass in DL1 and that associated with the overshoot effect are $\sim 0.9 \times 10^7 M_\odot$ and $\gtrsim 1.8 \times 10^7 M_\odot$ (Table 1), respectively. The result indicates that most of the accretion gas does not enter the CMZ directly but rather overshoots into the bar channel on the other side. Based on our observations, the current inflow efficiency can be easily obtained to be $\sim 1/3$ on average, which agrees well with the simulation (e.g., Hatchfield et al. 2021). Considering the importance of the overshoot effect (e.g., Maciejewski et al. 2002; Sormani & Barnes 2019; Hatchfield et al. 2021), we estimate an average inflow rate as $\gtrsim 1/3 \times 2 \times (0.9 \times 10^7 M_\odot / 24 \text{ Myr} + 1.8 \times 10^7 M_\odot / 15 \text{ Myr}) \gtrsim 1.1 M_\odot \text{ yr}^{-1}$. Here, $1/3$ is the observed inflow efficiency, while 2 corresponds to both the near and far bars. And 15 Myr comes from the gas kinematics of the DL2 and DL3 inflows by adopting an average inflow velocity of $\sim 90 - 100 \text{ km s}^{-1}$ (see DL2

and DL3 in Figure 1). Note that the instantaneous accretion rate can be several times higher than the average value. For example, it can easily cause the accretion rate to increase by nearly five times as several MCs (e.g., with a mass of $\sim 10^5 M_\odot$ and a size of ~ 10 pc) with low angular momentum (and thus higher inflow efficiency than $1/3$) settle into the CMZ within $\lesssim 0.1$ Myr. The gas accumulated in the G3/G5/G7 regions serves as a potential reservoir to regulate the instantaneous gas inflow rate.

Again, not all bar-driven gas flows directly enter the CMZ; instead, they take approximately three orbital periods to settle into the CMZ (i.e., the observed small inflow efficiency of $\sim 1/3$). Through this process, the gas is subjected to intense gravitational torques from the bar, causing it to be stretched, distorted, shredded, torn apart, and fragmented (Figure 2(c)). Apparently, the overshoot effect greatly lengthens the action time of various dynamical processes before the accretion gas enters the CMZ. Throughout the entire dynamical process, the angular momentum of the gas changes and redistributes due to the combined effects such as torque interactions from the bar, inelastic cloud–cloud collisions, gas viscosity, and various instabilities. The shock dissipation generated during the sufficient dynamics will redistribute angular momentum outward. This enables the distorted gas flows to efficiently transport material from kiloparsec scales to regions within a few hundred parsecs of the GC while also supporting the scenario of the periodic migration of gas toward the CMZ.

Briefly, the confirmation of the overshoot gas, together with frequent collisions caused by intersecting flows, provides detailed observational evidence to explain the dynamics of gas flows toward the CMZ. The overshoot gas with lower angular momentum gradually converges into the bar channel, then flows toward the CMZ again

(see DL2 and DL3 in Figure 3). Because of the overshoot effect and frequent collisions, the accretion gas is able to efficiently transfer its excess angular momentum outward through various dynamical processes and then cause the gas to gradually flow toward the CMZ. Here, the gravitational torque of the robust rotating Galactic bar makes a large contribution in the process of redistributing the gas and removing angular momentum from the molecular gas that eventually settles into the CMZ. Due to the interaction of various torques with viscous gas and the frequent collisions between gas flows, at the same time, the strong DISSIPATION process is also essential for the effective outward transfer of gas angular momentum, which in turn remarkably regulates the gas flow dynamics and gas accumulation in the CMZ over the secular evolution of the Galaxy.

4. LARGE-SCALE TILTED GAS FLOWS AND THE TWISTED ∞ STRUCTURE IN THE CMZ

The tilted dust lane has been discussed in many works (e.g., Liszt 2006, 2008; Rodriguez-Fernandez et al. 2006; Marshall et al. 2008; Sormani & Barnes 2019; Tress et al. 2020; Akhter et al. 2021). We also confirm that the near dust lane DL1 with a length of $\sim 3.2\text{--}3.4$ kpc exhibits distorted features during the large-scale gas accretion driven by the Galactic bar. Additionally, DL1 is distinctly located below the Galactic plane, which is exactly the opposite of the gas flow of the far dust lane above the plane (see Figure 3).

Our previous studies showed that the slightly tilted midplane to the IAU-defined plane (i.e., $b = 0^\circ$, see Figure 7 in Su et al. 2016) is caused by the Sun’s height above the physical midplane of the Milky Way (i.e., $z_{\text{sun}} \sim 15\text{--}17$ pc; see Su et al. 2016, 2019, 2021). However, the tilted large-scale gas flows toward the CMZ cannot be explained by this (e.g., see discussions in Bland-Hawthorn & Gerhard 2016) because the maxi-

mum deviation of the CO gas structure reaches $\lesssim -170$ pc (or $b \lesssim -1.5^\circ$ at $l \sim +5.5^\circ$) from the Galactic plane of $b = 0^\circ$. The deviation value is about 2 times larger than the thickness of the thin CO disk (see Table 3 in Su et al. 2021). Considering the smaller thickness of the molecular gas disk in the inner 3–4 kpc region, this deviation from the $b = 0^\circ$ plane is even more severe. We attribute the large-scale gas flows to a true tilted feature relative to the Galactic midplane. Based on our CO data and model (Su et al. 2024), the tilted angle of the bar lanes relative to the Galactic midplane in $l = [+6^\circ, -4^\circ]$ is estimated to be $\theta_{\text{bar lanes}} \gtrsim 5^\circ$, which roughly agrees with the simulations (e.g., $\sim 0^\circ - 5^\circ$ in Tress et al. 2020). Indeed, the gas structure revealed by the HI emission exhibits a more extreme tilted characteristic (i.e., $b \lesssim -3.5^\circ$ or $z_{\text{gas}} \lesssim -350$ pc for the atomic gas with the most negative velocity; see Burton & Liszt 1983).

The vertical distribution of gas (e.g., the tilted and warped gas flows) is modulated by the strong gravitational torque generated by the rotating bar and various dissipative forces. In our observation, the gravitational potential of the bar can effectively trap the gas flows into the dust lane (Figure 3). The gas on different orbits is perturbed by the nonaxisymmetric gravitational potential, leading it to undergo non-circular motion around the GC and oscillations relative to the bar. Due to the varying torque exerted by the bar’s potential on the gas, gas flowing along different trajectories and inclinations will move with varying precession rates until it eventually settles into the bar’s potential, aligns with the bar’s major axis, and then rotates around the GC with the bar. These torques also induce misalignments across different parts of the bar lanes. When gas flows on different orbits are subjected to varying torques, they develop distorted or warped structures as observed in CO data. In the process, the angular momentum of the overshoot flows is also

transferred to the bar through the dynamic friction. Alternatively, the distortion of the bar lanes caused by resonant trapping of x_1 orbits (e.g., Lokas 2019) may also influence the distribution and motion of the gas. The ongoing interaction between the gas flows and the bar itself accumulates over time, continuously affecting the bar’s structure and motion as it gains mass and angular momentum by exerting torque on the gas.

The above processes are accompanied by complex dynamical interactions that alter the angular momentum and motion states of the gas flows. We confirmed that collisions between gas flows are frequent during the dynamical processes in the G3, G5, and G7 regions. On the one hand, the nonaxisymmetric bar decouples the gas inflows from their initial dynamical state, resulting in rapid assimilation of the accretion gas into the bar potential (e.g., DL2 and DL3). On the other hand, the frequent collisions between gas flows (G3 and G5), combined with the tangential shear of the tidal forces exerted by the nonaxisymmetric bar, result in significant dissipation in the twisted gas flows. Indeed, the typical timescale of these dissipative processes, which are driven by shocks and strong turbulence, may be comparable to the short dynamical timescales associated with gas flow collisions. During the dynamical process of overshoot gas settling into the Galactic bar potential, the dissipation from collisions between misaligned gas flows, together with gas viscosity and the effects of various torques, serves as an efficient mechanism for the outward transfer of angular momentum of gas, thus facilitating their gradual migration toward the CMZ.

The scenario is strongly supported by our observations that the overshoot gas is not fully relaxed into the Galactic bar potential. That is, the overshoot gas from the far dust lane exhibits a more tilted structure (i.e., ~ 1.5 times larger; see $b \lesssim -1.8$ from $l \sim +3^\circ$ to $+11^\circ$ in

Figure 2(c)) than the near dust lane DL1 below the Galactic plane, while a portion of the gas passing through the bar channel even extends above the Galactic plane (i.e., DL2 is above and almost parallel to the Galactic plane). The distorted or warped gas structures in observations may represent the oscillatory characteristics of gas flows perpendicular to the Galactic bar as it moves and relaxes in the bar potential.

Meanwhile, the motion state of the self-consistent bar evolves over time through the exchange of angular momentum between the bar itself and the accreted material. As a result, the bar gains angular momentum from the captured gas and loses it to the halo and the outer stellar disk (e.g., Queiroz et al. 2021; Wylie et al. 2022; Dillamore et al. 2023), leading to a gradual change in the state of the bar (e.g., the morphology, structure, and kinematics; see Li et al. 2016; Chiba et al. 2021; Clarke & Gerhard 2022; Lucey et al. 2023; Vislosky et al. 2024). We suggest that the nonaxisymmetric bar is essential for regulating the redistribution of accreted gas and its angular momentum transfer. This self-regulating process may stably maintain large-scale gas accretion and gas recirculation over a considerable timescales in the presence of the bar (e.g., $\sim 4\text{--}8$ Gyr, see Bovy et al. 2019; Nepal et al. 2024).

The accumulated gas in the CMZ inherits the information of the gas supplied by the large-scale inflows, which includes the fresh gas from the disk at $R_{GC} \sim 3\text{--}4$ kpc (with higher angular momentum but lower accretion rate) and the recycled gas from the overshoot effect (with lower angular momentum but a higher accretion rate). The moving direction of the large-scale inflows (DL1) is well consistent with the trend of the ∞ structure at the far side of the CMZ (see the red solid arrow in the CMZ of Figure 3). That is, gas along the DL1 moves from the negative latitude at $l \sim +0.8$ toward the positive latitude at $l \sim -0.4$, and then back down toward the

negative latitude (e.g., see [Molinari et al. 2011](#); [Lipman et al. 2024](#); [Veena et al. 2024](#); [Walker et al. 2024](#); [Károly et al. 2025](#)).

Simultaneously, the inflowing gas along the far dust lane moves from the positive latitude to the negative latitude at $l \sim -0^\circ.6$, then toward the positive latitude at $l \sim +0^\circ.7$, and finally back down toward the negative latitude again (i.e., the near side of the CMZ; see the blue solid arrow in the CMZ of Figure 3). Similar to the previous discussion, when the gas flows pass near the x2 orbit, not all gas directly enters the CMZ; instead, some gas experiences the overshoot effect because of its higher angular momentum. Our data have clearly demonstrated that the overshoot gas flew past the near side of the CMZ and then collided violently with the inflowing gas from the DL2 and DL3 (i.e., see the G3 region in Figure 2(b); also see clouds studied by [Busch et al. 2022](#)).

We thus propose that the twisted ∞ feature of the CMZ (e.g., [Molinari et al. 2011](#); [Kruijssen et al. 2015](#); [Ridley et al. 2017](#)) arises from the combined effects of the large-scale tilted gas flows in the dust lanes and the locally distorted gas structure dominated by the strong gravitational potential within a few hundred parsecs of GC (i.e., the nuclear stellar disk; see [Sormani et al. 2022](#)). The orbit periods of the twisted ∞ structure of the CMZ are about 2–4 Myr ([Molinari et al. 2011](#); [Kruijssen et al. 2015](#)), suggesting a rapid precession of the gas under the influence of external nonaxisymmetric gravitational potential and the large-scale tilted gas inflows (e.g., [Tress et al. 2020](#)). The timescale of several million years mentioned above is consistent with the dynamical time (2–3 Myr) of gas inflow from the G3 region into the CMZ, indicating that external gas input significantly shapes the geometric configuration and dynamic properties of the CMZ (e.g., local gas accumulation, twisted structure, and rapid precession). Recent observations have revealed that the molec-

ular circumnuclear disks with different kinematics are misaligned with the large-scale gas structure ([Combes et al. 2019](#); [Ruffa et al. 2019, 2020](#); [Papachristou et al. 2023](#)), indicating that highly warped gas structures are likely prevalent in the central region of galaxies.

The dynamical processes in the inner Galaxy cause gas flows to exchange mass and angular momentum with their surroundings, enabling the CMZ to gain fresh gas from the Galactic disk and the recycled gas from the overshoot effect. Given the long-term accretion process and the remarkable transient accretion effects caused by overshooting, the nonuniform accumulation of gas (e.g., the instantaneous accretion rate of about $5\text{--}10\ M_\odot\text{yr}^{-1}$) can significantly feed and regulate star formation in the CMZ. Due to the highly distorted and inhomogeneous nature of gas inflows, the accretion process onto the CMZ, and even onto the SMBH, is likely highly nonuniform. This could result in the ∞ ring of the CMZ and jets of the SMBH exhibiting strong precession and intermittent variability. Furthermore, feedback from star formation in the CMZ and the SMBH (e.g., [Emsellem et al. 2015](#); [Kruijssen et al. 2015](#); [Krumholz et al. 2017, 2018](#); [Armillotta et al. 2019](#); [Anderson et al. 2020](#); [Sormani et al. 2020](#); [Tress et al. 2020](#); [Martínez-Arranz et al. 2024](#); [Takekawa et al. 2024](#)) contributes to reducing the angular momentum of gas in the CMZ, enabling a fraction of lower angular momentum gas to migrate further toward the region closer to the GC and thereby increasing the potential activities of the SMBH.

In simple terms, the gas and star-forming environment in the CMZ can be regulated by both the external gas input through the bar channel (this work) and the various feedback therein (e.g., [Heywood et al. 2019](#); [Ponti et al. 2021](#); [Mackey et al. 2024](#); [Nogueras-Lara 2024](#); [Nonhebel et al. 2024](#); [Sarkar 2024](#)), thus achieving a delicate balance between gas fuel supply and

star formation in the extreme environments. Under the control of nonaxisymmetric gravitational potential of the Galactic bar, the continuous accumulations of gas with VARYING inflow rates, along with frequent interactions between gas flows and star formation, can exist simultaneously within a few hundred parsecs of the GC over a long timescale. This is what distinguishes the CMZ from other star-forming regions on the Galactic disk.

5. SUMMARY

Based on CO morphological and kinematic details revealed by the MWISP data, we investigate the nature of the approaching and receding gas flows toward the CMZ. Our main results are as follows.

1. The MWISP CO data show that a large-scale gas structure, characterized by highly negative velocities, is composed of many filamentary MCs and is moving toward the observer (Figure 1). Based on the observations, for the first time, we have demonstrated that the overshoot gas from the far dust lane coexists with the near dust lane at an similar inclination angle to that of the Galactic bar ($\phi_{\text{bar}} = 23^\circ \pm 3^\circ$, see details in [Su et al. 2024](#)). The overshoot effect is critical in regulating the secular dynamical evolution of gas cycles in the inner Galaxy.

2. The overshoot clouds are decelerating (G7), reaccelerating (G5), and eventually converging near the bar channel (i.e., DL1 with a cross-sectional diameter of ~ 320 pc). Undoubtedly, a substantial amount of molecular gas is constantly changing its state of motion and spiraling toward the CMZ due to the gravitational potential of the bar. The total mass of the gas with lower angular momentum, and related to the overshoot effect, is about 2 times that of the fresh gas accreted directly from the Galactic disk at $R_{\text{GC}} \sim 3\text{--}4$ kpc (Table 1). This

indicates an average inflow efficiency of $1/3$ for the current period.

3. The cloud–cloud collision features between the overshoot gas from the far dust lane and the gas inflows toward the CMZ are clearly evident in the G3 and G5 regions (Figure 2; see details in Section 2). Other interaction features between gas flows and the Galactic bar are also well illustrated, such as changes in gas distribution and kinematics, shearing/nonrelaxed gas features relative to the bar, frequent collisions and convergence between clouds with different trajectories, and distorted bar lanes, etc.

4. As one of the most important gas components, molecular gas undergoes nonnegligible DISSIPATION processes due to strong turbulence. During various dynamical processes, including frequent inelastic collisions, viscosity between gas flows, and shear from the bar’s torque, the angular momentum of the gas is efficiently reduced (i.e., DL2+DL3 vs. DL1 in Section 3). These processes collectively facilitate the inward migration of molecular gas in the x1 orbit, ultimately settling the gas with lower angular momentum into the x2 orbit (i.e., the CMZ) over a few tens of Myr.

5. The overshoot flows exhibit a more pronounced tilted feature compared to the near dust lane. We suggest that the twisted ∞ structure in the CMZ ([Molinari et al. 2011](#)) originates from the combined effects of the tilted gas flows on kiloparsec scales and the local warped gas structure dominated by the strong gravitational potential of the nuclear stellar disk. The nonaxisymmetric gravitational potential of the Galactic bar serves as an effective regulator of angular momentum redistribution, mass transport, and the secular evolution of the inner Galaxy (see Section 4).

6. The gas inflow rate toward the CMZ is $\gtrsim 1.1 M_{\odot} \text{ yr}^{-1}$ according to the total gas input from the fresh gas of the near dust lane and the overshoot gas from the far dust lane. The average gas inflow rate toward the CMZ is roughly comparable to the outflow's rate for the Galactic nuclear winds (Su et al. 2022). However, the gas inflow rate exhibits periodic variations of several Myr due to the overshoot effect (also refer to Hatchfield et al. 2021) and significant instantaneous fluctuations (e.g., ~ 5 – 10 times higher than the average gas inflow rate) due to gas accumulation in some regions (e.g., G3 at $R_{\text{GC}} \sim \frac{1}{7} R_{\text{bar}}$, G5 at $R_{\text{GC}} \sim \frac{1}{2} R_{\text{bar}}$, and G7 at $R_{\text{GC}} \sim \frac{2}{3} R_{\text{bar}}$).

7. The MWISP survey with the high-sensitivity and high-velocity resolution can dramatically enhance our ability to capture the detailed morphology and kinematics of gas flows toward the CMZ, helping us to reconstruct the entire dynamical evolution of gas flows within ~ 3 – 4 kpc of the GC (Figure 3). Large-scale gas accretion and overshoot effects, combined with various feedback within a few hundred parsecs of the GC, jointly shape the gas distribution, physical properties, and dynamical evolution of the CMZ, as well as the subsequent star formation processes therein.

The holistic structure and large-sample statistical properties revealed by the observations are important for our understanding of the gas dynamics toward the center of galaxies. Moreover, many simulation studies have been done to explain how gas structures form within a bar and how they depend on various bar param-

eters (e.g., the bar strength, the effective sound speed, the pattern speed of the bar, the inclination angle of the bar, the magnetic field, the various gravitational potentials, etc.; see Lindblad et al. 1996; Kim et al. 2012a,b; Kim & Stone 2012; Feng et al. 2024; Sormani et al. 2024; Tress et al. 2024). The comprehensive analysis of large-scale survey data, combined with the comparison of observational features and model simulations, is essential for accurately understanding the astrophysical phenomena and fundamental physical processes that dominate galaxy evolution.

ACKNOWLEDGMENTS

We would like to thank the referee for several constructive comments that led to improvements in the paper. This research made use of the data from the Milky Way Imaging Scroll Painting (MWISP) project, which is a multiline survey in $^{12}\text{CO}/^{13}\text{CO}/\text{C}^{18}\text{O}$ along the northern Galactic plane with the PMO-13.7m telescope. We are grateful to all the members of the MWISP working group, particularly the staff members at the PMO-13.7m telescope, for their long-term support. MWISP was sponsored by National Key R&D Program of China with grants 2023YFA1608000 and 2017YFA0402701 and by CAS Key Research Program of Frontier Sciences with grant QYZDJ-SSW-SLH047. We also acknowledge support from the National Natural Science Foundation of China through grants 12173090 and 12041305.

Facility: PMO:DLH

REFERENCES

- | | |
|---|---|
| <p>Akhter, S., Cunningham, M. R., Harvey-Smith, L., et al. 2021, MNRAS, 502, 5896,
doi: 10.1093/mnras/staa267</p> | <p>Anderson, L. D., Sormani, M. C., Ginsburg, A., et al. 2020, ApJ, 901, 51,
doi: 10.3847/1538-4357/abaddf6</p> |
|---|---|

- Armillaotta, L., Krumholz, M. R., Di Teodoro, E. M., & McClure-Griffiths, N. M. 2019, MNRAS, 490, 4401, doi: [10.1093/mnras/stz2880](https://doi.org/10.1093/mnras/stz2880)
- Athanassoula, E. 1992, MNRAS, 259, 345, doi: [10.1093/mnras/259.2.345](https://doi.org/10.1093/mnras/259.2.345)
- Battersby, C., Walker, D. L., Barnes, A., et al. 2024, arXiv e-prints, arXiv:2410.17334, <https://arxiv.org/abs/2410.17334>
- Bland-Hawthorn, J., & Gerhard, O. 2016, ARA&A, 54, 529, doi: [10.1146/annurev-astro-081915-023441](https://doi.org/10.1146/annurev-astro-081915-023441)
- Bolatto, A. D., Wolfire, M., & Leroy, A. K. 2013, ARA&A, 51, 207, doi: [10.1146/annurev-astro-082812-140944](https://doi.org/10.1146/annurev-astro-082812-140944)
- Bovy, J., Leung, H. W., Hunt, J. A. S., et al. 2019, MNRAS, 490, 4740, doi: [10.1093/mnras/stz2891](https://doi.org/10.1093/mnras/stz2891)
- Bryant, A., & Krabbe, A. 2021, NewAR, 93, 101630, doi: [10.1016/j.newar.2021.101630](https://doi.org/10.1016/j.newar.2021.101630)
- Burton, W. B., & Liszt, H. S. 1983, A&AS, 52, 63
- Busch, L. A., Riquelme, D., Güsten, R., et al. 2022, A&A, 668, A183, doi: [10.1051/0004-6361/202244870](https://doi.org/10.1051/0004-6361/202244870)
- Butterfield, N., Morgan, L., Barnes, A., et al. 2025, arXiv e-prints, arXiv:2503.14174, <https://arxiv.org/abs/2503.14174>
- Chaves-Velasquez, L., Gómez, G. C., & Pérez-Villegas, Á. 2025, PASA, 42, e014, doi: [10.1017/pasa.2024.130](https://doi.org/10.1017/pasa.2024.130)
- Chiba, R., Friske, J. K. S., & Schönrich, R. 2021, MNRAS, 500, 4710, doi: [10.1093/mnras/staa3585](https://doi.org/10.1093/mnras/staa3585)
- Clarke, J. P., & Gerhard, O. 2022, MNRAS, 512, 2171, doi: [10.1093/mnras/stac603](https://doi.org/10.1093/mnras/stac603)
- Combes, F., García-Burillo, S., Casasola, V., et al. 2014, A&A, 565, A97, doi: [10.1051/0004-6361/201423433](https://doi.org/10.1051/0004-6361/201423433)
- Combes, F., García-Burillo, S., Audibert, A., et al. 2019, A&A, 623, A79, doi: [10.1051/0004-6361/201834560](https://doi.org/10.1051/0004-6361/201834560)
- Dahmen, G., Huttemeister, S., Wilson, T. L., & Mauersberger, R. 1998, A&A, 331, 959, doi: [10.48550/arXiv.astro-ph/9711117](https://doi.org/10.48550/arXiv.astro-ph/9711117)
- Dame, T. M., Hartmann, D., & Thaddeus, P. 2001, ApJ, 547, 792, doi: [10.1086/318388](https://doi.org/10.1086/318388)
- Dame, T. M., & Thaddeus, P. 2008, ApJL, 683, L143, doi: [10.1086/591669](https://doi.org/10.1086/591669)
- Dillamore, A. M., Belokurov, V., Evans, N. W., & Davies, E. Y. 2023, MNRAS, 524, 3596, doi: [10.1093/mnras/stad2136](https://doi.org/10.1093/mnras/stad2136)
- Eden, D. J., Moore, T. J. T., Currie, M. J., et al. 2020, MNRAS, 498, 5936, doi: [10.1093/mnras/staa2734](https://doi.org/10.1093/mnras/staa2734)
- Emsellem, E., Renaud, F., Bournaud, F., et al. 2015, MNRAS, 446, 2468, doi: [10.1093/mnras/stu2209](https://doi.org/10.1093/mnras/stu2209)
- Englmaier, P., & Gerhard, O. 1999, MNRAS, 304, 512, doi: [10.1046/j.1365-8711.1999.02280.x](https://doi.org/10.1046/j.1365-8711.1999.02280.x)
- Enokiya, R., Torii, K., & Fukui, Y. 2021, PASJ, 73, S75, doi: [10.1093/pasj/psz119](https://doi.org/10.1093/pasj/psz119)
- Feng, Z.-X., Li, Z., Shen, J., et al. 2024, ApJ, 963, 22, doi: [10.3847/1538-4357/ad13ee](https://doi.org/10.3847/1538-4357/ad13ee)
- Ferrière, K., Gillard, W., & Jean, P. 2007, A&A, 467, 611, doi: [10.1051/0004-6361:20066992](https://doi.org/10.1051/0004-6361:20066992)
- Fukui, Y., Habe, A., Inoue, T., Enokiya, R., & Tachihara, K. 2021, PASJ, 73, S1, doi: [10.1093/pasj/psaa103](https://doi.org/10.1093/pasj/psaa103)
- Furukawa, N., Dawson, J. R., Ohama, A., et al. 2009, ApJL, 696, L115, doi: [10.1088/0004-637X/696/2/L115](https://doi.org/10.1088/0004-637X/696/2/L115)
- Fux, R. 1999, A&A, 345, 787, doi: [10.48550/arXiv.astro-ph/9903154](https://doi.org/10.48550/arXiv.astro-ph/9903154)
- Gong, Y., Fang, M., Mao, R., et al. 2017, ApJL, 835, L14, doi: [10.3847/2041-8213/835/1/L14](https://doi.org/10.3847/2041-8213/835/1/L14)
- Gramze, S. R., Ginsburg, A., Meier, D. S., et al. 2023, ApJ, 959, 93, doi: [10.3847/1538-4357/ad01be](https://doi.org/10.3847/1538-4357/ad01be)
- Hatchfield, H. P., Sormani, M. C., Tress, R. G., et al. 2021, ApJ, 922, 79, doi: [10.3847/1538-4357/ac1e89](https://doi.org/10.3847/1538-4357/ac1e89)
- Henshaw, J. D., Barnes, A. T., Battersby, C., et al. 2023, in Astronomical Society of the Pacific Conference Series, Vol. 534, Protostars and Planets VII, ed. S. Inutsuka, Y. Aikawa, T. Muto, K. Tomida, & M. Tamura, 83, doi: [10.48550/arXiv.2203.11223](https://doi.org/10.48550/arXiv.2203.11223)
- Henshaw, J. D., Ginsburg, A., Haworth, T. J., et al. 2019, MNRAS, 485, 2457, doi: [10.1093/mnras/stz471](https://doi.org/10.1093/mnras/stz471)
- Heywood, I., Camilo, F., Cotton, W. D., et al. 2019, Nature, 573, 235, doi: [10.1038/s41586-019-1532-5](https://doi.org/10.1038/s41586-019-1532-5)
- Hilmi, T., Minchev, I., Buck, T., et al. 2020, MNRAS, 497, 933, doi: [10.1093/mnras/staa1934](https://doi.org/10.1093/mnras/staa1934)
- Inoue, T., & Fukui, Y. 2013, ApJL, 774, L31, doi: [10.1088/2041-8205/774/2/L31](https://doi.org/10.1088/2041-8205/774/2/L31)
- Karoly, J., Ward-Thompson, D., Pattle, K., et al. 2025, ApJL, 982, L22, doi: [10.3847/2041-8213/adbc67](https://doi.org/10.3847/2041-8213/adbc67)

- Kim, W.-T., Seo, W.-Y., & Kim, Y. 2012a, *ApJ*, 758, 14, doi: [10.1088/0004-637X/758/1/14](https://doi.org/10.1088/0004-637X/758/1/14)
- Kim, W.-T., Seo, W.-Y., Stone, J. M., Yoon, D., & Teuben, P. J. 2012b, *ApJ*, 747, 60, doi: [10.1088/0004-637X/747/1/60](https://doi.org/10.1088/0004-637X/747/1/60)
- Kim, W.-T., & Stone, J. M. 2012, *ApJ*, 751, 124, doi: [10.1088/0004-637X/751/2/124](https://doi.org/10.1088/0004-637X/751/2/124)
- Koda, J., Scoville, N., & Heyer, M. 2016, *ApJ*, 823, 76, doi: [10.3847/0004-637X/823/2/76](https://doi.org/10.3847/0004-637X/823/2/76)
- Kohno, M., & Sofue, Y. 2024, *MNRAS*, 527, 9290, doi: [10.1093/mnras/stad3648](https://doi.org/10.1093/mnras/stad3648)
- Kruijssen, J. M. D., Dale, J. E., & Longmore, S. N. 2015, *MNRAS*, 447, 1059, doi: [10.1093/mnras/stu2526](https://doi.org/10.1093/mnras/stu2526)
- Kruijssen, J. M. D., Dale, J. E., Longmore, S. N., et al. 2019, *MNRAS*, 484, 5734, doi: [10.1093/mnras/stz381](https://doi.org/10.1093/mnras/stz381)
- Krumholz, M. R., Burkhardt, B., Forbes, J. C., & Crocker, R. M. 2018, *MNRAS*, 477, 2716, doi: [10.1093/mnras/sty852](https://doi.org/10.1093/mnras/sty852)
- Krumholz, M. R., Kruijssen, J. M. D., & Crocker, R. M. 2017, *MNRAS*, 466, 1213, doi: [10.1093/mnras/stw3195](https://doi.org/10.1093/mnras/stw3195)
- Kumar, J., Reid, M. J., Dame, T. M., et al. 2025, *ApJ*, 982, 185, doi: [10.3847/1538-4357/adb70f](https://doi.org/10.3847/1538-4357/adb70f)
- Launhardt, R., Zylka, R., & Mezger, P. G. 2002, *A&A*, 384, 112, doi: [10.1051/0004-6361:20020017](https://doi.org/10.1051/0004-6361:20020017)
- Leroy, A. K., Schinnerer, E., Hughes, A., et al. 2021, *ApJS*, 257, 43, doi: [10.3847/1538-4365/ac17f3](https://doi.org/10.3847/1538-4365/ac17f3)
- Li, Z., Gerhard, O., Shen, J., Portail, M., & Wegg, C. 2016, *ApJ*, 824, 13, doi: [10.3847/0004-637X/824/1/13](https://doi.org/10.3847/0004-637X/824/1/13)
- Lindblad, P. A. B., Lindblad, P. O., & Athanassoula, E. 1996, *A&A*, 313, 65
- Lipman, D., Battersby, C., Walker, D. L., et al. 2024, *arXiv e-prints*, arXiv:2410.17321, doi: [10.48550/arXiv.2410.17321](https://doi.org/10.48550/arXiv.2410.17321)
- Liszt, H. S. 2006, *A&A*, 447, 533, doi: [10.1051/0004-6361:20054070](https://doi.org/10.1051/0004-6361:20054070)
- . 2008, *A&A*, 486, 467, doi: [10.1051/0004-6361:200809748](https://doi.org/10.1051/0004-6361:200809748)
- Lokas, E. L. 2019, *A&A*, 629, A52, doi: [10.1051/0004-6361/201936056](https://doi.org/10.1051/0004-6361/201936056)
- Lucey, M., Pearson, S., Hunt, J. A. S., et al. 2023, *MNRAS*, 520, 4779, doi: [10.1093/mnras/stad406](https://doi.org/10.1093/mnras/stad406)
- Maciejewski, W., Teuben, P. J., Sparke, L. S., & Stone, J. M. 2002, *MNRAS*, 329, 502, doi: [10.1046/j.1365-8711.2002.04957.x](https://doi.org/10.1046/j.1365-8711.2002.04957.x)
- Mackey, S. C., Morris, M. R., Ponti, G., Anastasopoulou, K., & Mondal, S. 2024, *ApJL*, 966, L32, doi: [10.3847/2041-8213/ad3248](https://doi.org/10.3847/2041-8213/ad3248)
- Marshall, D. J., Fux, R., Robin, A. C., & Reylé, C. 2008, *A&A*, 477, L21, doi: [10.1051/0004-6361:20078967](https://doi.org/10.1051/0004-6361:20078967)
- Martínez-Arranz, A., Schödel, R., Nogueras-Lara, F., et al. 2024, *A&A*, 685, L7, doi: [10.1051/0004-6361/202449877](https://doi.org/10.1051/0004-6361/202449877)
- Molinari, S., Bally, J., Noriega-Crespo, A., et al. 2011, *ApJL*, 735, L33, doi: [10.1088/2041-8205/735/2/L33](https://doi.org/10.1088/2041-8205/735/2/L33)
- Nepal, S., Chiappini, C., Guiglion, G., et al. 2024, *A&A*, 681, L8, doi: [10.1051/0004-6361/202348365](https://doi.org/10.1051/0004-6361/202348365)
- Nilipour, A., Ott, J., Meier, D. S., et al. 2024, *ApJ*, 977, 37, doi: [10.3847/1538-4357/ad8631](https://doi.org/10.3847/1538-4357/ad8631)
- Nogueras-Lara, F. 2024, *A&A*, 681, L21, doi: [10.1051/0004-6361/202348712](https://doi.org/10.1051/0004-6361/202348712)
- Nonhebel, M., Barnes, A. T., Immer, K., et al. 2024, *A&A*, 691, A70, doi: [10.1051/0004-6361/202451190](https://doi.org/10.1051/0004-6361/202451190)
- Papachristou, M., Dasyra, K. M., Fernández-Ontiveros, J. A., et al. 2023, *A&A*, 679, A115, doi: [10.1051/0004-6361/202346464](https://doi.org/10.1051/0004-6361/202346464)
- Ponti, G., Morris, M. R., Churazov, E., Heywood, I., & Fender, R. P. 2021, *A&A*, 646, A66, doi: [10.1051/0004-6361/202039636](https://doi.org/10.1051/0004-6361/202039636)
- Queiroz, A. B. A., Chiappini, C., Perez-Villegas, A., et al. 2021, *A&A*, 656, A156, doi: [10.1051/0004-6361/202039030](https://doi.org/10.1051/0004-6361/202039030)
- Regan, M. W., & Teuben, P. J. 2004, *ApJ*, 600, 595, doi: [10.1086/380116](https://doi.org/10.1086/380116)
- Reid, M. J., Dame, T. M., Menten, K. M., & Brunthaler, A. 2016, *ApJ*, 823, 77, doi: [10.3847/0004-637X/823/2/77](https://doi.org/10.3847/0004-637X/823/2/77)
- Reid, M. J., Menten, K. M., Brunthaler, A., et al. 2019, *ApJ*, 885, 131, doi: [10.3847/1538-4357/ab4a11](https://doi.org/10.3847/1538-4357/ab4a11)
- Ridley, M. G. L., Sormani, M. C., Treß, R. G., Magorrian, J., & Klessen, R. S. 2017, *MNRAS*, 469, 2251, doi: [10.1093/mnras/stx944](https://doi.org/10.1093/mnras/stx944)
- Riener, M., Kainulainen, J., Henshaw, J. D., et al. 2019, *A&A*, 628, A78, doi: [10.1051/0004-6361/201935519](https://doi.org/10.1051/0004-6361/201935519)
- Rodriguez-Fernandez, N. J., & Combes, F. 2008, *A&A*, 489, 115, doi: [10.1051/0004-6361:200809644](https://doi.org/10.1051/0004-6361:200809644)

- Rodriguez-Fernandez, N. J., Combes, F., Martin-Pintado, J., Wilson, T. L., & Apponi, A. 2006, *A&A*, 455, 963, doi: [10.1051/0004-6361:20064813](https://doi.org/10.1051/0004-6361:20064813)
- Ruffa, I., Laing, R. A., Prandoni, I., et al. 2020, *MNRAS*, 499, 5719, doi: [10.1093/mnras/staa3166](https://doi.org/10.1093/mnras/staa3166)
- Ruffa, I., Davis, T. A., Prandoni, I., et al. 2019, *MNRAS*, 489, 3739, doi: [10.1093/mnras/stz2368](https://doi.org/10.1093/mnras/stz2368)
- Sarkar, K. C. 2024, *A&A Rv*, 32, 1, doi: [10.1007/s00159-024-00152-1](https://doi.org/10.1007/s00159-024-00152-1)
- Schinnerer, E., & Leroy, A. K. 2024, *ARA&A*, 62, 369, doi: [10.1146/annurev-astro-071221-052651](https://doi.org/10.1146/annurev-astro-071221-052651)
- Schinnerer, E., Emsellem, E., Henshaw, J. D., et al. 2023, *ApJL*, 944, L15, doi: [10.3847/2041-8213/acac9e](https://doi.org/10.3847/2041-8213/acac9e)
- Schuller, F., Urquhart, J. S., Csengeri, T., et al. 2021, *MNRAS*, 500, 3064, doi: [10.1093/mnras/staa2369](https://doi.org/10.1093/mnras/staa2369)
- Schultheis, M., Chen, B. Q., Jiang, B. W., et al. 2014, *A&A*, 566, A120, doi: [10.1051/0004-6361/201322788](https://doi.org/10.1051/0004-6361/201322788)
- Shen, J., & Zheng, X.-W. 2020, *Research in Astronomy and Astrophysics*, 20, 159, doi: [10.1088/1674-4527/20/10/159](https://doi.org/10.1088/1674-4527/20/10/159)
- Sheth, K., Vogel, S. N., Regan, M. W., Thornley, M. D., & Teuben, P. J. 2005, *ApJ*, 632, 217, doi: [10.1086/432409](https://doi.org/10.1086/432409)
- Simion, I. T., Belokurov, V., Irwin, M., et al. 2017, *MNRAS*, 471, 4323, doi: [10.1093/mnras/stx1832](https://doi.org/10.1093/mnras/stx1832)
- Sormani, M. C., & Barnes, A. T. 2019, *MNRAS*, 484, 1213, doi: [10.1093/mnras/stz046](https://doi.org/10.1093/mnras/stz046)
- Sormani, M. C., Binney, J., & Magorrian, J. 2015, *MNRAS*, 449, 2421, doi: [10.1093/mnras/stv441](https://doi.org/10.1093/mnras/stv441)
- Sormani, M. C., Sobacchi, E., & Sanders, J. L. 2024, *MNRAS*, 528, 5742, doi: [10.1093/mnras/stae082](https://doi.org/10.1093/mnras/stae082)
- Sormani, M. C., Tress, R. G., Glover, S. C. O., et al. 2020, *MNRAS*, 497, 5024, doi: [10.1093/mnras/staa1999](https://doi.org/10.1093/mnras/staa1999)
- Sormani, M. C., Treß, R. G., Glover, S. C. O., et al. 2019, *MNRAS*, 488, 4663, doi: [10.1093/mnras/stz2054](https://doi.org/10.1093/mnras/stz2054)
- Sormani, M. C., Sanders, J. L., Fritz, T. K., et al. 2022, *MNRAS*, 512, 1857, doi: [10.1093/mnras/stac639](https://doi.org/10.1093/mnras/stac639)
- Sormani, M. C., Barnes, A. T., Sun, J., et al. 2023, *MNRAS*, 523, 2918, doi: [10.1093/mnras/stad1554](https://doi.org/10.1093/mnras/stad1554)
- Stark, A. A., & Bania, T. M. 1986, *ApJL*, 306, L17, doi: [10.1086/184695](https://doi.org/10.1086/184695)
- Strong, A. W., Moskalenko, I. V., Reimer, O., Digel, S., & Diehl, R. 2004, *A&A*, 422, L47, doi: [10.1051/0004-6361:20040172](https://doi.org/10.1051/0004-6361:20040172)
- Stuber, S. K., Schinnerer, E., Williams, T. G., et al. 2023, *A&A*, 676, A113, doi: [10.1051/0004-6361/202346318](https://doi.org/10.1051/0004-6361/202346318)
- Su, Y., Sun, Y., Li, C., et al. 2016, *ApJ*, 828, 59, doi: [10.3847/0004-637X/828/1/59](https://doi.org/10.3847/0004-637X/828/1/59)
- Su, Y., Yang, J., Zhang, S., et al. 2019, *ApJS*, 240, 9, doi: [10.3847/1538-4365/aaf1c8](https://doi.org/10.3847/1538-4365/aaf1c8)
- Su, Y., Yang, J., Yan, Q.-Z., et al. 2021, *ApJ*, 910, 131, doi: [10.3847/1538-4357/abe5ab](https://doi.org/10.3847/1538-4357/abe5ab)
- Su, Y., Zhang, S., Yang, J., et al. 2022, *ApJ*, 930, 112, doi: [10.3847/1538-4357/ac63b3](https://doi.org/10.3847/1538-4357/ac63b3)
- Su, Y., Zhang, S., Sun, Y., et al. 2024, *ApJL*, 971, L6, doi: [10.3847/2041-8213/ad656d](https://doi.org/10.3847/2041-8213/ad656d)
- Takekawa, S., Oka, T., Tsujimoto, S., et al. 2024, *ApJL*, 972, L3, doi: [10.3847/2041-8213/ad6c51](https://doi.org/10.3847/2041-8213/ad6c51)
- Tokuyama, S., Oka, T., Takekawa, S., et al. 2019, *PASJ*, 71, S19, doi: [10.1093/pasj/psy150](https://doi.org/10.1093/pasj/psy150)
- Tress, R. G., Sormani, M. C., Glover, S. C. O., et al. 2020, *MNRAS*, 499, 4455, doi: [10.1093/mnras/staa3120](https://doi.org/10.1093/mnras/staa3120)
- Tress, R. G., Sormani, M. C., Girichidis, P., et al. 2024, *A&A*, 691, A303, doi: [10.1051/0004-6361/202450035](https://doi.org/10.1051/0004-6361/202450035)
- Veena, V. S., Kim, W. J., Sánchez-Monge, Á., et al. 2024, *A&A*, 689, A121, doi: [10.1051/0004-6361/202450902](https://doi.org/10.1051/0004-6361/202450902)
- Vislosky, E., Minchev, I., Khoperskov, S., et al. 2024, *MNRAS*, 528, 3576, doi: [10.1093/mnras/stae083](https://doi.org/10.1093/mnras/stae083)
- Walker, D. L., Battersby, C., Lipman, D., et al. 2024, *arXiv e-prints*, arXiv:2410.17320, doi: [10.48550/arXiv.2410.17320](https://doi.org/10.48550/arXiv.2410.17320)
- Wallace, J., Battersby, C., Mills, E. A. C., et al. 2022, *ApJ*, 939, 58, doi: [10.3847/1538-4357/ac951a](https://doi.org/10.3847/1538-4357/ac951a)
- Wang, C., Feng, H., Yang, J., et al. 2023, *AJ*, 166, 121, doi: [10.3847/1538-3881/acebdd](https://doi.org/10.3847/1538-3881/acebdd)
- Wegg, C., Gerhard, O., & Portail, M. 2015, *MNRAS*, 450, 4050, doi: [10.1093/mnras/stv745](https://doi.org/10.1093/mnras/stv745)
- Wheeler, A., Abril-Cabezas, I., Trick, W. H., Frangkoudi, F., & Ness, M. 2022, *ApJ*, 935, 28, doi: [10.3847/1538-4357/ac7da0](https://doi.org/10.3847/1538-4357/ac7da0)
- Whitmore, B. C., Chandar, R., Rodríguez, M. J., et al. 2023, *ApJL*, 944, L14, doi: [10.3847/2041-8213/aca94](https://doi.org/10.3847/2041-8213/aca94)

- Williams, B. A., Walker, D. L., Longmore, S. N.,
et al. 2022, MNRAS, 514, 578,
doi: [10.1093/mnras/stac1378](https://doi.org/10.1093/mnras/stac1378)
- Wylie, S. M., Clarke, J. P., & Gerhard, O. E.
2022, A&A, 659, A80,
doi: [10.1051/0004-6361/202142343](https://doi.org/10.1051/0004-6361/202142343)
- Zhang, H., Belokurov, V., Evans, N. W., Kane,
S. G., & Sanders, J. L. 2024a, MNRAS, 533,
3395, doi: [10.1093/mnras/stae2023](https://doi.org/10.1093/mnras/stae2023)
- Zhang, S., Su, Y., Chen, X., et al. 2024b, AJ, 167,
220, doi: [10.3847/1538-3881/ad2fcb](https://doi.org/10.3847/1538-3881/ad2fcb)

Table 1. Parameters of MC Samples toward the CMZ

Name	Number ^a	T_{peak12}^b (K)	T_{peak13}^b (K)	$v(\text{FWHM})^b$ (km s ⁻¹)	$\frac{I_{13\text{CO}}}{I_{12\text{CO}}}^b$	X_{CO}^c ($\times 10^{20}$ cm ⁻² (K km s ⁻¹) ⁻¹)	MC Mass ^d ($\times 10^6 M_\odot$)	Total Gas Mass ($\times 10^6 M_\odot$)
DL1	64	8.7 \pm 3.2	3.5 \pm 1.8	15.5 \pm 4.3	0.14 \pm 0.04	0.9 \pm 0.4	5.6 \pm 2.4	$\sim 9.0 \pm 3.3^e$
Intermediate ^f	93	9.4 \pm 3.7	4.3 \pm 2.2	18.1 \pm 6.0	$\lesssim 0.17 \pm 0.04^g$	1.2 \pm 0.5	10.0 \pm 4.3	$\gtrsim 17.0 \pm 7.3^h$
Overshoot	13	5.5 \pm 2.0	1.6 \pm 0.3	10.3 \pm 3.2	0.10 \pm 0.02	0.7 \pm 0.3	0.2 \pm 0.1	$\gtrsim 0.9 \pm 0.3^i$

NOTE— ^a Here we only list the numbers of the large-scale MC samples with an angular size > 50 arcmin².

^b Statistics from ¹²CO flux-weighted MC samples.

^c X_{CO} is derived from the ¹²CO and ¹³CO emission of the large-scale MCs (i.e., $N(\text{H}_2) \approx 7 \pm 3 \times 10^5 \times N(^{13}\text{CO})$; see the details in Su et al. 2024).

^d The total mass of the large-scale MCs is calculated from the estimated CO-to-H₂ conversion factor.

^e The total gas mass is calculated from the CO-to-H₂ conversion factor for all identified MCs along the near dust lane. The contribution from the corresponding H I gas, accounting for $\sim 15\%$ of the molecular gas mass, has been included in the calculations of the total gas mass.

^f MCs with v_{LSR} between the DL1 and the overshoot gas (Figure 1). Note that some MC samples from the blended regions have been excluded, so the reported MC mass is a lower limit. These MCs may also include a small portion of the fresh gas in DL1 due to interactions between gas flows in the bar channel.

^g The total emission of ¹³CO is calculated from the l - b - v space of the fitted ¹²CO cloud. The measurement of $I_{13\text{CO}}$ can be contaminated with unrelated gas emission due to the complicated velocity components toward the large MCs. Consequently, the ratio reported here is only an upper limit.

^h Because of the confusion from foreground MCs near the Galactic plane, only some of small-scale MCs associated with the shock regions, such as G3, G5, DL2, and DL3, are considered here and are conservatively estimated to account for $\gtrsim 70\%$ of the total mass of the large-scale MCs.

ⁱ The small MCs dominate the mass in the region, and the contribution of the corresponding H I gas accounts for $\gtrsim 50\%$ of the total molecular gas mass.

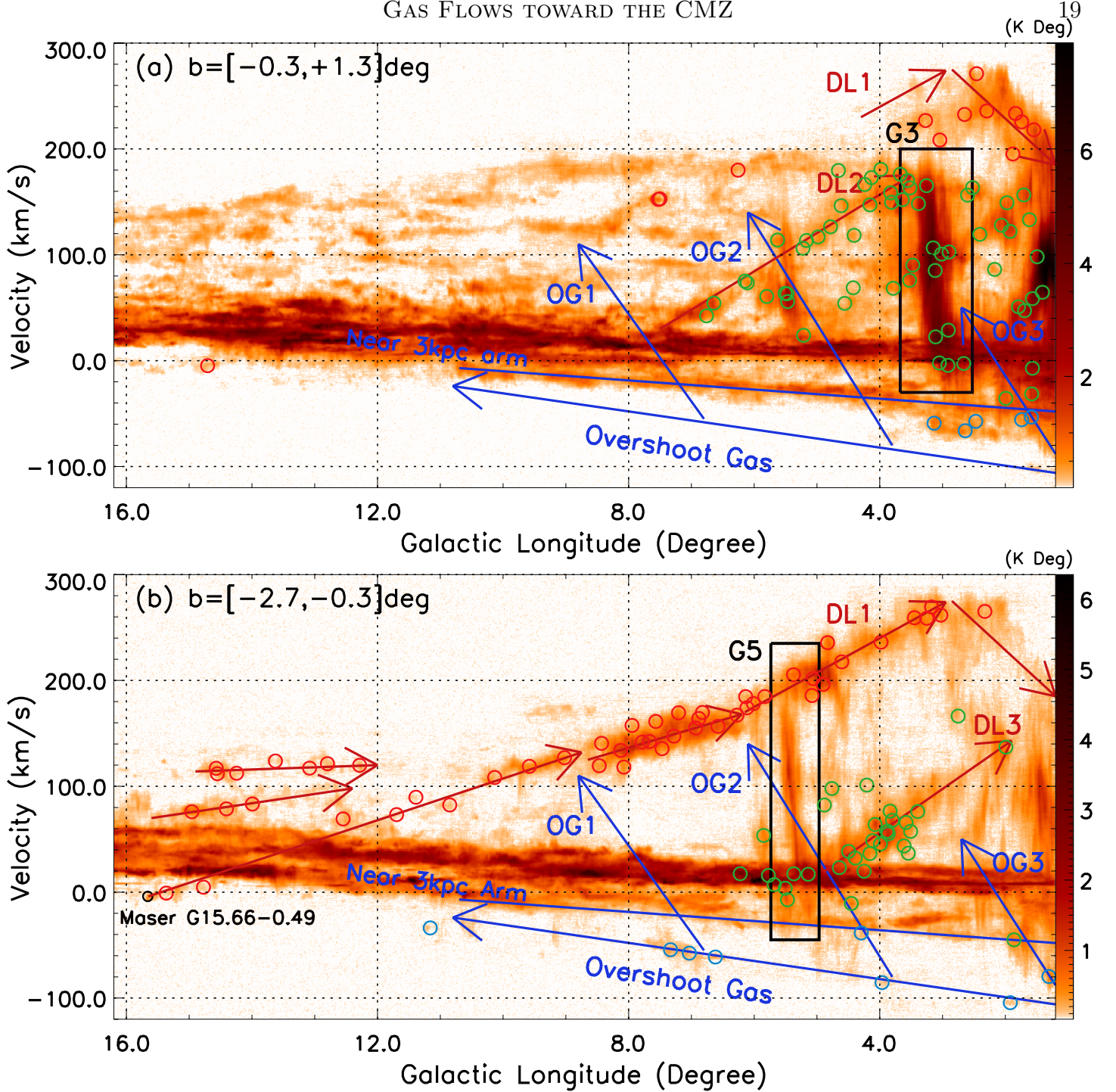


Figure 1. Longitude–velocity diagram of ^{12}CO emission from the MWISP survey (Su et al. 2019) on a $0.5'$ grid along $l = 16^\circ 2' - 1^\circ 2'$. The upper panel shows the l – v features averaged over $-0^\circ 3' \leq b \leq +1^\circ 3'$, while the lower panel displays the main structure of the near dust lane over $-2^\circ 7' \leq b \leq -0^\circ 3'$. The markers represent the different parts of the near dust lane (red arrows for main near dust lane DL1, and two other components of DL2 and DL3), the overshoot gas from the far dust lane (blue arrows), and the near 3 kpc arm (blue line; see text and also refer to Figure 3 in Su et al. 2024). The rectangles show the extended velocity features of G3 (or Bania 2 in Stark & Bania 1986) and G5 (Gramze et al. 2023). The red, green, and blue circles represent the three categories of MC samples with an angular size $> 50 \text{ arcmin}^2$ as listed in Table 1. The maser G015.66-00.49 (at a parallax of $0.22 \pm 0.029 \text{ mas}$ and $v_{\text{LSR}} = -4 \text{ km s}^{-1}$; Reid et al. 2019) is also labeled in the figure.

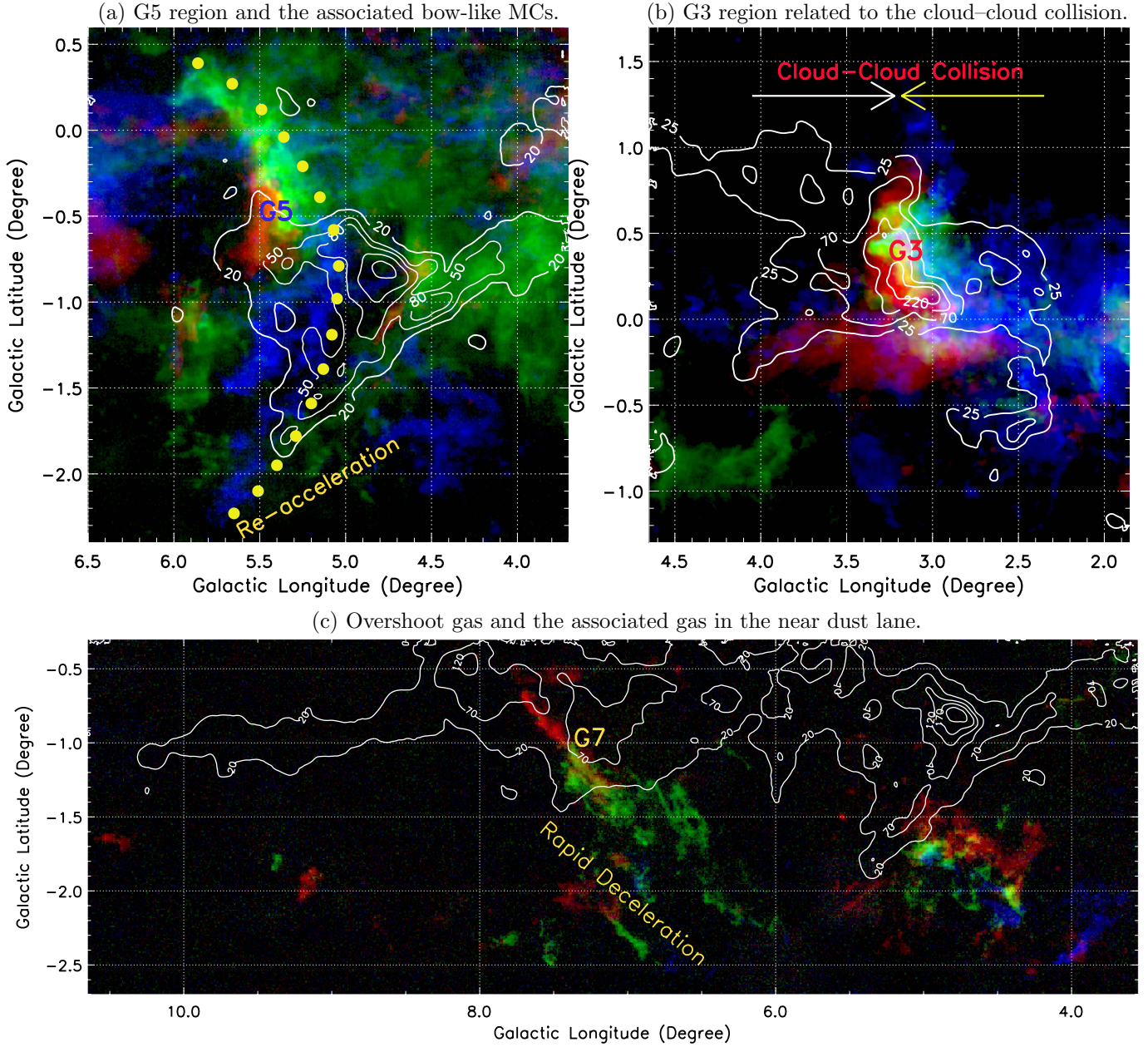
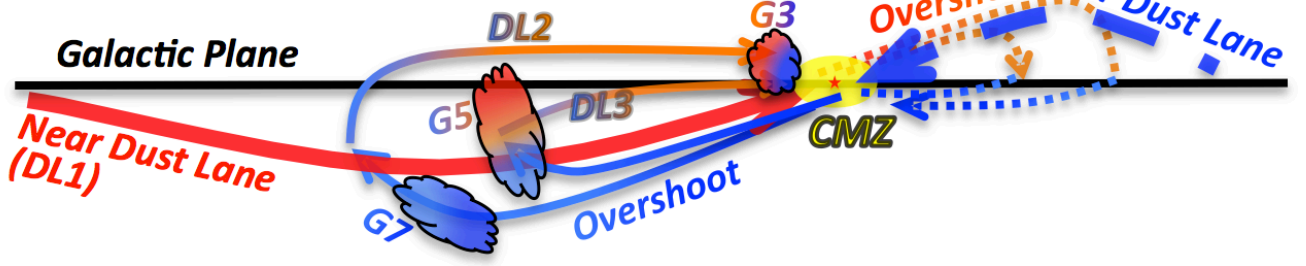


Figure 2. Three cases for the physical association between the molecular gas in the near dust lane and the overshoot gas from the far dust lane. Panel (a) illustrates bow-like MCs that are spatially coherent over a wide range of velocities ($[-25, -5] \text{ km s}^{-1}$ for blue, $[+27, +80] \text{ km s}^{-1}$ for green, $[+120, +170] \text{ km s}^{-1}$ for red, and $[+180, +240] \text{ km s}^{-1}$ for white contours). The large-scale shock structure traced by CO emission is indicated by a yellow dotted line. The G5 region at ($l \sim 5^\circ.4$, $b \sim -0^\circ.4$) or $R_{\text{GC}} \sim 1.6 \text{ kpc}$ is labeled on the figure. Panel (b) shows the cloud-cloud collision between the approaching gas from the overshoot effect ($[-20, +5] \text{ km s}^{-1}$ for blue, $[+25, +60] \text{ km s}^{-1}$ for green, and $[+80, +120] \text{ km s}^{-1}$ for red) and the receding gas along the DL2 ($[+130, +180] \text{ km s}^{-1}$ for white contours). The G3 region at ($l \sim 3^\circ.2$, $b \sim 0^\circ.3$) or $R_{\text{GC}} \sim 0.5 \text{ kpc}$ is labeled on the figure. Panel (c) shows the spatial correlation between the overshoot gas ($[-105, -70] \text{ km s}^{-1}$ for blue, $[-70, -55] \text{ km s}^{-1}$ for green, and $[-55, -40] \text{ km s}^{-1}$ for red) and the DL1 (white contours for the near dust lane; also refer to Figure 1 in Su et al. 2024). The G7 region at ($l \sim 7^\circ.3$, $b \sim -1^\circ.1$) or $R_{\text{GC}} \sim 2.2 \text{ kpc}$ is labeled on the figure. White contours in the three panels mark different levels of the integrated CO intensity in K km s^{-1} .

(a) Edge-on view



(b) Face-on view

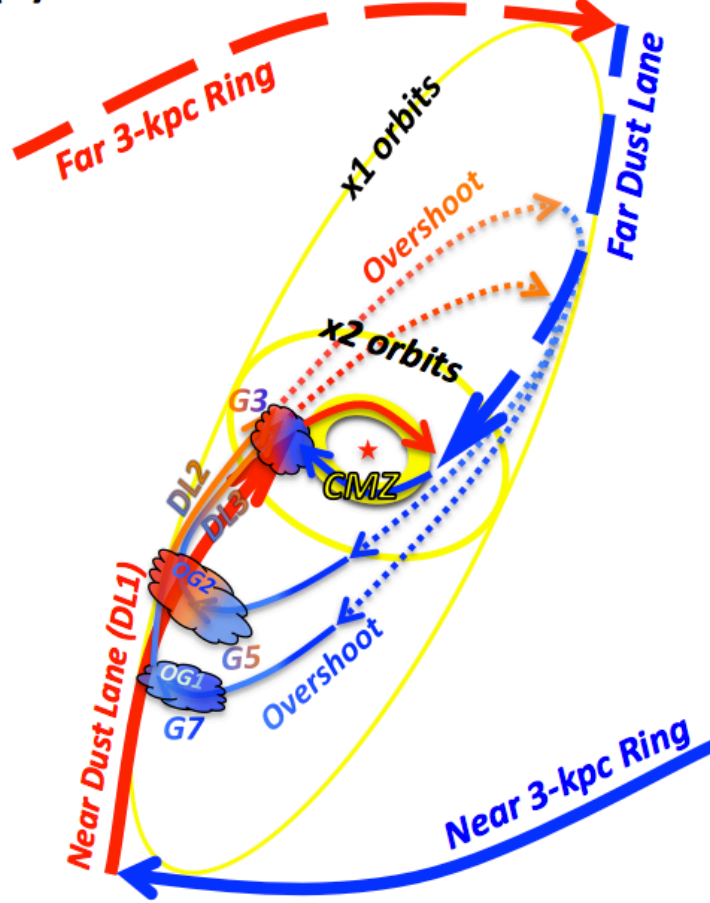


Figure 3. Holistic perspective of the large-scale molecular gas flows toward the CMZ based on the MWISP CO data and other supplementary data. In the diagram, the upper portion displays an edge-on view (from the Sun) of the identified gas structures and some prominent features by considering the observation effect (e.g., see Figure 2 in Gramze et al. 2023), while the lower portion shows a face-on view of the corresponding structures. Note that the b scale (the Galactic latitude) has been enlarged to better show the twisted or warped structure of the gas flows. The parameters of the geometry are from Su et al. (2024), i.e., the inclination angle of $\phi_{\text{bar}} = 23^\circ \pm 3^\circ$, the bar length of $\sim 3.2 - 3.4$ kpc, and the tilted angle of $\theta_{\text{bar lanes}} \gtrsim 5^\circ$ for the large-scale gas feature from $l \sim +6^\circ$ to -4° . Here we adopt $R_0 = 8.15$ kpc (Reid et al. 2019). Solid lines represent the near-side gas flows from the MWISP observations, while dotted lines show the far-side gas flows based on other CO surveys and the mirrored MWISP data. Dominated by the nonaxisymmetric gravitational potential of the Galactic bar, the overshoot effect plays a crucial role in redistributing angular momentum outward through various dynamical processes such as shocks generated by bar perturbations, frequent inelastic collisions, and nonnegligible viscosity. G5 and G7 are located near the $R_{\text{GC}} \sim \frac{1}{2}R_{\text{bar}}$ and $R_{\text{GC}} \sim \frac{2}{3}R_{\text{bar}}$ regions, respectively. OG1 and OG2 (see Figure 1) in the map roughly show the trajectory of the gas flows from approaching to receding. As a result, a large amount of molecular gas located several kiloparsecs away can efficiently migrate into regions within a few hundred parsecs of the GC over a few tens of millions of years, leading to a burst of star formation in the CMZ and facilitating the growth of the central SMBH.